Journal of Nuclear Medicine, published on August 26, 2021 as doi:10.2967/jnumed.121.262500

Biodistribution of ^{18}F-FES in patients with metastatic ER+ breast cancer undergoing treatment with Rintodestrant (G1T48), a novel selective estrogen receptor degrader

Ramsha Iqbal[1], Maqsood Yaqub[2], Daniela E. Oprea-Lager[2], Yeukman Liu[1], Anne Marije Luik[1], Andy P. Beelen[3], Robert C. Schuit[2], Albert D. Windhorst[2], Ronald Boellaard[2], Catharina W. Menke-van der Houven van Oordt[1]

[1] *Amsterdam UMC, Vrije Universiteit Amsterdam, Medical Oncology, Cancer Center Amsterdam, De Boelelaan 1117, Amsterdam, Netherlands*

[2] *Amsterdam UMC, Vrije Universiteit Amsterdam, Radiology and Nuclear Medicine, Cancer Center Amsterdam, De Boelelaan 1117, Amsterdam, Netherlands*

[3] *G1 Therapeutics Inc., Research Triangle Park, North Carolina, USA*

Corresponding author

R. Iqbal, MD

Department of Medical Oncology

Amsterdam University Medical Centers – location VU University Medical Center

De Boelelaan 1117, 1081 HV Amsterdam, The Netherlands

Telephone: +31-20-4441050 / Fax number: +31-20-4444355

E-mail: r.iqbal@amsterdamumc.nl / ORCID: https://orcid.org/0000-0002-5382-0112

Words: 5218.

Running title: Biodistribution of ^{18}F-FES

Abstract

16α-^{18}F-fluoro-17β-estradiol (^{18}F-FES) is a positron emission tomography (PET) tracer characterizing the expression of the estrogen receptor (ER). As therapy can interfere with the kinetics and biodistribution of ^{18}F-FES, the aim of this study was to describe the biodistribution of ^{18}F-FES in patients with metastatic ER+ breast cancer undergoing treatment with rintodestrant (G1T48), a novel selective ER degrader.

Methods: Eight patients underwent ^{18}F-FES PET/CT imaging at baseline, 4-6 weeks during treatment with rintodestrant (interim) and after treatment. After intravenous administration of 200 MBq (+/- 10%) ^{18}F-FES, a 50-min dynamic PET/CT scan of the thorax was performed, followed by a whole body PET/CT scan 60 min post-injection. Blood samples were drawn for measuring whole blood and plasma activity concentration and the parent fraction of ^{18}F-FES. Volumes of interest (VOIs) were placed in the aorta ascendens and in healthy tissues on both dynamic and whole body PET scans. Standard uptake values (SUVs) and target-to-blood ratios (TBR) were calculated. Area under the curves (AUCs) of input functions and time-activity curves were calculated as a measure of uptake in different regions.

Results: ^{18}F-FES concentration in whole blood (and plasma) significantly (P <0.05) increased at interim with median AUCs of 96.6, 116.6 and 110.3 at baseline, interim and after treatment, respectively. In ER expressing tissues, i.e. the uterus and the pituitary gland, both SUV and TBR showed high ^{18}F-FES uptake at baseline, followed by a decrease in uptake at interim (uterus: SUV -50.6% and TBR -58.5%, pituitary gland: SUV -39.0% and TBR -48.3%) which tended to return to baseline values after treatment (uterus: SUV -21.5% and TBR -37.9%, pituitary gland: SUV -14.2% and TBR -26.0%, compared to baseline). In other healthy tissues, tracer uptake remained stable over the 3 time-points.

Conclusion: The biodistribution of ^{18}F-FES is altered in blood and in ER expressing healthy tissues during therapy with rintodestrant. This indicates that rintodestrant alters the kinetics of the tracer which could affect interpretation and quantification of ^{18}F-FES uptake. Of note, ≥6 days after ending treatment with rintodestrant, the biodistribution returned to baseline values, consistent with recovery of ER availability after wash-out of the drug.

Keywords: ^{18}F-FES, PET, estrogen receptor, breast cancer, biodistribution

Introduction

Estrogen receptor positive (ER+) breast cancer is the most common diagnosed breast cancer type among women worldwide (*1*,*2*). Patients with ER+ tumors can be treated with ER-targeted therapy, also known as endocrine therapy. Endocrine therapies include selective estrogen receptor modifiers (SERMs) and degraders (SERDs) (*3*). These therapies decrease ER availability by binding to the ER to interfere with estrogen binding and/or degrading the ER, thus effectively eliminating ER expression.

The most frequently prescribed SERD in clinical practice is fulvestrant. However, its use is compromised by its poor bioavailability coupled with its intramuscular route of administration. Therefore, novel oral SERDs are being developed, including rintodestrant (G1T48) which can be administered at (relatively) higher doses with less patient discomfort (*4*).

For effective treatment of patients it is important to accurately describe and evaluate the mode of action of these novel ER-targeted therapies. Positron emission tomography/computed tomography (PET/CT) using ER-targeting tracers, such as 16α-^{18}F--fluoro-17β-estradiol (^{18}F-FES), is a promising approach to investigate this (*5*,*6*). ^{18}F-FES uptake, as measured 60 min after tracer administration using standardized uptake values (SUVs), correlates strongly with ERα expression (as compared to ER expression in tumor biopsies) with overall sensitivity and specificity of 84% [95% CI 73-91%] and 98% [95% CI 90-100%], respectively (*7*). In addition to clinical studies to identify patients likely to respond to endocrine therapy, ^{18}F-FES PET appears to be an interesting tool for response prediction and dose finding for (novel) SERMs or SERDs (*3*,*5*,*8-12*). For patients receiving SERMs or SERDs, such as tamoxifen or fulvestrant, respectively, it is known that a decrease in ^{18}F-FES uptake after start of therapy correlates with response to these drugs (*10*,*12*). In addition, this during therapy ^{18}F-FES PET imaging strategy can also help in dose finding studies with novel ER-targeting drugs to establish the optimal dose to achieve maximum ER blockade (*7*).

However, to reliably assess changes in ER availability during endocrine therapy, it is essential to investigate the biodistribution of the tracer, i.e. its uptake in blood pool and healthy tissues (with and without target expression) under various conditions (with and without therapy). In case this changes during treatment, one can conclude that the given therapy interferes with the kinetics of the tracer. Therefore, the aim of this prospective sub-study was to describe the biodistribution of the ^{18}F-FES tracer in patients with metastatic ER+ breast cancer undergoing treatment with rintodestrant.

Materials & Methods

Post-menopausal female patients with histologically proven metastatic ER+/HER2- breast cancer were prospectively included in this study (sub-study of a phase I trial: NCT03455270) at the Amsterdam University Medical Centers – location VUmc. Patients had progressive disease after having received a maximum of 3 lines of cytotoxic chemotherapy and 3 lines of endocrine therapy in the metastatic setting. Patients were excluded when they received treatment with estrogen receptor modulators (i.e. tamoxifen or fulvestrant) ≤5 weeks prior to inclusion as these drugs interfere with the availability of ER. All patients provided written informed consent in accordance with the regulations of the Medical Ethics Review Committee (METc number: 2018/085) of the Universitair Medisch Centrum Groningen.

Treatment. Eligible patients received rintodestrant orally once a day. A 3+3 dose escalation design was used to determine the recommended phase 2 dose (based on the pharmacokinetic, anti-tumor activity and toxicity profile of the drug) (*4*). The starting dose in the first cohort was 200 mg which could be escalated each time with 200 mg in the following cohorts, i.e. cohort 2 - 400 mg, cohort 3 - 600 mg etcetera. The dose could be maximally escalated up to 2000 mg/day. Patients will receive rintodestrant until clinically or radiographically progressive disease has been determined or there is unacceptable toxicity.

PET imaging. PET scans were performed on an Ingenuity TF PET/CT scanner (Philips Medical Systems, Cleveland, Ohio, USA). Patients underwent dynamic and whole body ^{18}F-FES PET/CT imaging at 3 different time-points: at baseline, 4 weeks during treatment with rintodestrant (interim) and after treatment (scans were performed within 10 days of the last dose of rintodestrant). All patients were instructed to fast for 4 h before the start of the scan to avoid high tracer uptake in the hepatobiliary and gastro-intestinal tract as this is the metabolization and elimination route of the tracer. For each scan, patients received two venous cannulae, one for tracer injection and one for blood sampling. First, a low-dose CT scan of the thorax was performed for attenuation correction. Next, a 50-min dynamic ^{18}F-FES PET scan of the thorax (18.4 cm axial field of view) was performed, starting directly after intravenous administration of 200 (±10%) MBq ^{18}F-FES. Subsequently, a whole body low-dose CT scan was performed for attenuation correction, followed by a whole body ^{18}F-FES PET scan at 60 min post-injection (skull vertex to mid-thigh) with 2-3 min/bed position depending on patient weight (2 min: for 61-90 kg and 3 min: for >90 kg).

PET data were normalized and corrected for dead time, randoms, scatter and decay. In combination with CT-based attenuation correction, both scans provided images with a final voxel size of 4×4×4 mm^3 and a spatial resolution of 5–7 mm in full width at half maximum. Dynamic PET scans were reconstructed using a 3-dimensional row action maximum likelihood reconstruction algorithm (3D-RAMLA) (*13*) into 27 frames (1x10s, 4x5s, 3x10s, 3x20s, 2x30s, 7x60s, 2x150s, 3x300s, 2x600s). The whole body scans were reconstructed using the BLOB-OS-TF reconstruction algorithm (*14*).

Blood sampling. Prior to tracer administration, a venous blood sample was taken to determine estradiol and sex-hormone binding globuline (SHBG) levels, as these could potentially affect ^{18}F-FES uptake (*15*). After tracer administration, venous blood samples were collected at 5, 10, 20, 30, 40, 55 and ±90 min post-injection. Before each sample, 2-5 mL blood was drawn, followed by drawing a 7 mL sample and flushing of the cannula with 2.5 mL of saline afterwards.

Blood was collected in a heparin tube and centrifuged for 5 minutes at 4000 revolutions per minute (Hettich universal 16, Depex B.V., the Netherlands). Plasma was separated from blood cells and 1 mL was diluted with 2 ml of 0.15M HCl and loaded onto an activated tC2 Sep-Pak cartridge (Waters, the Netherlands). The solid phase extraction was washed with 5 mL of water. These combined fractions were defined as the polar radiolabeled metabolite. Thereafter, the tC18 Sep-Pak cartridge was eluted with 1.5 mL of methanol followed by 1.5 ml of water. This eluate was defined as the non-polar fraction and was analyzed using high-performance liquid chromatography. The stationary phase was a Phenomenex Gemini C18, 10*250 mm, 5 um and the mobile phase was acetonitril/0.1% ammonium acetate in a mixture of 55/45 at a flow of 3 ml/min.

Whole blood and plasma activity concentration and the parent fraction of ^{18}F-FES were measured. These data were used to correct the image derived (whole blood) input function to acquire a metabolite corrected plasma input function (described in the paragraph below).

Data-analysis: dynamic and whole body ^{18}F-FES PET data. Volumes of interests (VOIs) were defined on PET and CT images using in-house developed software (Accurate tool, R. Boellaard) (*16*). For the whole body scans, fixed size spherical VOIs with a diameter of 1, 2 or 4 cm (depending on the size of the organ) were placed in various

healthy organs, i.e. white matter in brain, pituitary gland, lung, breast, bone, muscle, liver, spleen, subcutaneous fat, kidney and the uterus. Furthermore, if applicable up to 5 metastatic bone lesions were defined using a 40% iso-contour of the max voxel value (*17*). PET activity concentration from these VOIs, both averaged standardized uptake values (SUVs) and target-to-blood ratios (TBRs) were calculated according to equations 1 and 2, respectively.

$$SUV = \frac{activity\ concentration\ VOI\ (kBq/mL)}{administered\ dose\ (MBq)\ /\ patient\ weight\ (kg)} \quad \text{Eq. 1}$$

$$TBR = \frac{activity\ concentration\ target\ (kBq/mL)}{activity\ concentration\ blood\ (kBq/mL)} \quad \text{Eq. 2}$$

Fixed size VOIs were also defined in healthy organs that were visible on the dynamic ^{18}F-FES scans, i.e. lung, breast, bone, muscle and liver. For these VOIs, time-activity curves (TACs) were generated which were corrected for administered dose and body weight to generate SUV curves.

Image derived input functions (IDIFs) were generated from dynamic ^{18}F-FES scans, using the early frames (0-2.5 min) in which the first pass of the bolus was best visualized. A fixed size VOI of 1.5 cm was placed in 5 consecutive axial planes within the lumen of the ascending aorta on the PET scan. The low-dose CT scan was used as a reference for anatomical localization. These VOIs were then projected onto all image frames to generate a whole blood IDIF. All IDIFs were calibrated using the radioactivity concentrations in the venous blood samples. In addition, IDIFs were corrected for both plasma-to-blood ratios and metabolites to obtain metabolite corrected plasma input functions. Furthermore, SUV input curves were generated by normalizing the IDIFs for administered dose and body weight. The area under the input curves (AUCs) was calculated to more precisely describe the uptake over the duration of the dynamic scan.

Statistical analysis. Statistical analyses were performed using SPSS Statistics 26 (IBM Corp., Armonk, N.Y., USA). For blood sampling data, tracer uptake in blood pool and healthy organs, median and interquartile ranges (IQR) were reported. For assessing changes in clinical parameters and tracer uptake in blood pool and healthy organs between the various scanning time-points, the Wilcoxon signed rank test was used (paired testing). Differences were considered significant for a *P*-value <0.05 for observing trends in data.

Results

Patients. Eight female patients with metastatic ER+ breast cancer with an average (±SD) age of 63 (±7.35) years (*Supplemental Table 1*) were included. Patients received various doses of rintodestrant depending on the cohort they were included in, ranging from 400 mg to 1000 mg per day (*Supplemental Table 1 and 2*). A total of 20 dynamic and whole body ^{18}F-FES PET/CT scans were performed and evaluable: 8 scans were performed at baseline, 7 scans at interim and 5 scans after treatment. All patients scanned after treatment had discontinued treatment due to progressive disease with an average (±SD) treatment duration of 4.5 (±2.6) months (*Supplemental Table 1*). After treatment, 3 scans were performed ≤2 days and 2 scans were performed ≥6 days after end of treatment (EoT)). For 2 patients, the interim scans were performed at 6 weeks (instead of 4 weeks) due to logistical issues.

The median (IQR) injected ^{18}F-FES doses were 187 (181-196), 187 (180-195) and 183.2 (177.4-188.2) MBq (Wilcoxon test, P >0.23) at baseline, interim and after treatment, respectively. Median (IQR) body weight at baseline, interim and after treatment was 77 (65-105), 81 (66-114) and 81 (64-108), respectively (*Supplemental Table 2*). Body weight decreased significantly (max. decrease in weight: 7.4%) between baseline and after treatment (P = 0.04). This was accompanied by a significant increase in total body fat between baseline and after treatment (P = 0.04) – with total body fat volume (in L) of 28.1 (19.2-43.6), 32.1 (19.5-50.0) and 32.2 (18.8-52.1) at baseline, interim and after treatment. However, the percentage injected dose of ^{18}F-FES in total body fat did not vary over the various time-points (P >0.05) with values of 24.2% (19.7-28.4), 26.2% (20.9-31.4) and 24.2% (18.9-31.6) at baseline, interim and after treatment.

Blood sampling. Blood sampling data showed that median (IQR) estradiol levels in blood showed no difference over the various time-points (P >0.18), whereas SHBG levels changed after start of therapy: 66.5 (26.0-121.5), 95.0 (45.0-232.0) and 97.0 (53.0-210.0) nmol/L at baseline, interim and after treatment, respectively. This showed a significant increase in values between baseline and interim (P <0.02) and baseline and after treatment (P <0.04; *Supplemental Fig. 1*).

Blood sampling data (*Fig. 1*) showed that median whole blood activity concentrations, corrected for administered dose and patient weight, varied between a SUV of 1.4-1.5, 1.5-2.0 and 1.5-1.8 at baseline, interim and after treatment, respectively (*Fig. 1A*). SUV increased at interim and tended to normalize to baseline values after

treatment. The plasma-to-whole blood ratios remained constant over the 3 different time-points, ranging between 1.3-1.7 (*Fig. 1B*). The parent fraction of ^{18}F-FES in plasma showed a similar pattern over the 3 different time-points: a rapid decrease to ≈20% in the first 20 minutes post-injection (*Fig. 1C*) was observed. After the first 20 minutes, the parent fraction of ^{18}F-FES decreased quite slowly over time from 16 to 10%.

Tracer uptake in blood pool. Median (IQR) area under the curves (AUC) of the whole blood IDIFs (corrected for administered dose and body weight) at baseline, interim and after treatment were 96.6 (86.3-123.3), 116.6 (112.5-144.9) and 110.3 (97.9-132.1), respectively (*Fig. 2A, Supplemental Table 3*), showing increased levels of the tracer in blood at interim (Wilcoxon test, P <0.05). These findings were in accordance with the AUCs of the whole plasma IDIFs (*Fig. 2B, P <0.05*). Median AUCs of the metabolite corrected plasma input functions also showed an increase at interim: 54.6 (52.7-75.0), 63.6 (57.6-77.8) and 63.6 (53.4-90.9) at baseline, interim and after treatment (*Fig. 2C*). However, these differences at interim were not significant. For the whole blood, plasma and metabolite corrected plasma input curves, no differences in AUCs could be seen in patients scanned short vs late after EoT (*Supplemental Table 3*).

Visual assessment of ^{18}F-FES uptake. Using the whole body PET scans, ^{18}F-FES uptake in most healthy organs (except ER expressing tissues like the uterus and the pituitary gland) was visually similar at all the imaging time-points, with high tracer uptake in the liver, gallbladder, intestines, kidneys and bladder (*Fig. 3*). At baseline, high ^{18}F-FES uptake could be seen in the uterus and the pituitary gland which decreased at interim. However, ^{18}F-FES uptake could be seen again in patients scanned several days after EoT. Patients scanned short after EoT, showed similar uptake as seen at interim. In breast tissue, ^{18}F-FES uptake remained visually similar at all time-points.

Visual assessment of metastatic lesions showed ^{18}F-FES uptake at baseline in 6/8 patients. At interim, no lesions could be visualized in the 7/7 patients (*Fig. 3*). However, after treatment, lesions could be visualized again but only in patients scanned late after EoT (2/5 patients).

Quantification of ^{18}F-FES uptake. Using the dynamic scans, SUV TACs could be generated for healthy breast, lung, liver, muscle and bone as these were located in the field of view of the dynamic scan (*Fig. 4, Supplemental*

Table 4). For all these tissues, no changes in AUCs could be observed over the 3 different time-points (Wilcoxon test, $P > 0.05$).

Using whole body scans, tracer uptake in healthy tissues was assessed using SUV and TBR (*Supplemental Fig. 2 and 3*). For SUV and TBR, in most healthy tissues including bone, breast, kidney, liver, lung, muscle, subcutaneous fat and the spleen, ^{18}F-FES uptake remained similar over the 3 different scanning time-points. Quantification of tracer uptake in the uterus and the pituitary gland confirmed the qualitative findings: for both SUV and TBR ^{18}F-FES uptake decreased at interim (uterus: SUV -50.6% and TBR -58.5%, pituitary gland: SUV -39.0% and TBR -48.3%, compared to baseline). No correlation could be found between the various doses of rintodestrant that patients received and changes in tracer uptake in these tissues (Spearman's rho correlation, $P > 0.6$). This may suggest that even at the lowest dose, the blockade of these tissues was near 100% or at least sufficiently high to reduce ^{18}F-FES uptake below level of detection. Interestingly after treatment, ^{18}F-FES uptake increased to baseline values in patients scanned several days after EoT (uterus: SUV -2.4% and TBR -21.7%, pituitary gland: SUV -9.6% and TBR -12.0%, compared to baseline) whereas it remained reduced in patients scanned shortly after EoT (uterus: SUV -34.3% and TBR -48.7%, pituitary gland: SUV -30.0% and TBR -47.2%, compared to baseline).

At baseline, metastatic bone lesions showed significantly higher tracer uptake compared to healthy bone: median (IQR) SUV values of 1.6 (1.4-2.1) and 0.7 (0.5-0.8) and TBR values of 1.2 (1.1-1.6) and 0.5 (0.4-0.5) for lesions and healthy bone, respectively (*Supplemental Fig. 4*; $P < 0.003$). However, at interim, lesions could not be detected whereas tracer uptake in healthy bone could be quantified. After treatment, lesions could be visualized again but only in patients scanned late after EoT. Similar as baseline, these lesions showed high tracer uptake compared to healthy bone: SUV values of 1.9 (1.4-2.0) and 0.7 (0.7-0.8) and TBR values of 1.1 (0.8-1.2) and 0.5 (0.4-0.5) for lesions and healthy bone, respectively ($P < 0.003$).

Discussion

This study performed dynamic and whole body ^{18}F-FES PET/CT imaging at baseline, interim and after treatment to understand the effect of rintodestrant on the biodistribution of the ^{18}F-FES tracer.

Blood sampling and input data. Blood sampling and input data showed that whole blood and plasma activity concentrations of the tracer increased at interim and tended to return to baseline values after treatment. The increase in tracer activity concentrations is most likely the result of rintodestrant which interferes with ER availability for binding ^{18}F-FES (*4*). Therefore, more free tracer will be available in the circulation resulting in higher whole blood and plasma activity concentrations. However, other effects caused by the therapy could also potentially lead to these increased tracer concentrations in blood. We also found increased levels of SHBG. SHBG is a plasma glycoprotein that plays an important role in the transport and bioavailability of steroid hormones, including estradiol (*18*). It is known that therapies that increase the estradiol levels in circulation lead to an increase in SHBG levels (*19,20*). We did not observe a change in estradiol levels during therapy, however, it might be possible that the SHBG levels increased as a response to therapy with rintodestrant. Peterson et al (*15*). showed that SHBG levels are inversely associated with ^{18}F-FES uptake and subsequent higher levels of circulating ^{18}F-FES in blood, as also observed in our study.

The tracer metabolism was similar for all time-points. The parent fraction of ^{18}F-FES rapidly decreased in the first 20 min post-injection, indicating rapid metabolization of the tracer, in accordance with previous studies (*5,21*). After these 20 min, blood levels of radioactivity decreased quite slowly and/or remained fairly constant. Plasma to whole blood ratios were constantly high over time, for all 3 time-points. It is known that 35-45% of the ^{18}F-FES tracer is plasma protein-bound and that red cell binding is low which might explain these constant high ratios over time (*21*).

Visual assessment and quantification of ^{18}F-FES uptake in healthy tissues. As seen in previous publications, our study confirmed physiological high tracer uptake in the hepatobiliary, gastro-intestinal and urinary tract (*5,22*). This pattern was consistent over all time-points. Additionally, in metastatic lesions and in ER expressing healthy tissues (i.e. uterus and pituitary gland) high ^{18}F-FES uptake could be seen at baseline which is in accordance with previous studies (*22,23*). Tracer uptake decreased at interim, most likely due to the down regulatory effect of

rintodestrant and/or the ER-blocking effect of the drug. Interestingly, after treatment ^{18}F-FES uptake returned to near baselines levels, specifically in patients scanned late after EoT. In these cases, it is assumable that most of the administered drug is eliminated (half-life of rintodestrant: ≈16 hours) (*4*) and that the ERs in lesions and in the uterus and the pituitary gland are accessible for the tracer again. Indeed, in patients that were scanned shortly after EoT the uptake was still reduced, supporting that ER availability is still compromised due to the presence of the drug. These changes in ^{18}F-FES uptake could not be observed in breast tissue which is also known to have ER-expression. Breast tissue constantly showed low ^{18}F-FES uptake over the different time-points. Compared to other ER-expressing tissues for instance the uterus, the ER density in breast is significantly lower (*24*). Therefore, it can be expected that changes in uptake, potentially caused by therapy, are less prominent. In other healthy tissues, hardly any changes in tracer uptake could be detected, probably as in these tissues ER receptor expression is minimal or absent and thus the ^{18}F-FES uptake is aspecific (*24*,*25*).

For quantification of tracer uptake in healthy tissues at the various imaging time-points, AUCs of the SUV input functions (derived from the dynamic scans) and TBR and SUV (derived from the whole body scans) were used. In general, in all healthy tissues (except the uterus and the pituitary gland), AUCs, TBR and SUV showed that tracer uptake remained similar over the different time-points. TBR seems to be slightly more sensitive than SUV for assessing changes in biodistribution, probably as it also takes into account changes in tracer concentration in the blood pool (which do occur during therapy as can be seen in the sampling data and input functions).

Visualization of lesions was only possible at baseline and after treatment, the latter only in patients scanned late after EoT, most likely related to recovery of the ER-availability after wash-out of the drug as mentioned earlier. Overall, bone lesions showed higher ^{18}F-FES uptake than healthy bone. These lesions are expected to have high ER expression causing more targeted uptake of the tracer which is also more affected by ER degradation during treatment with rintodestrant. In healthy tissue the uptake is lower, consistent with aspecific uptake.

Limitations. Although the sample size may seem small, the strength of this study is that we collected dynamic and whole body scans at 3 time points per patient, allowing to directly compare changes in biodistribution in a repeated measure design within one patient. As we investigated tracer uptake in healthy tissues, we expect that there will be limited variation between patients which has been shown in similar previous PET biodistribution studies with

comparable small sample sizes and which is also found in our study. Besides, most quantitative PET study sample sizes are small, especially in case where an intensive scanning protocol is required, as was the case in this study.

Future directions. ^{18}F-FES imaging performed prior to start of therapy can identify ER+ disease to select patients for ER-targeted therapy. Complete blockage or degradation of the ER during treatment can be demonstrated by the absence of visual uptake in lesions. However, for quantification of more subtle changes in ^{18}F-FES uptake as a measure for ER availability and predictor of response to therapy with SERMs/SERDs, caution should be taken since our data shows that during therapy the kinetics and biodistribution of the tracer are altered which may affect interpretation.

Conclusion

The biodistribution of the ^{18}F-FES tracer is altered in blood and in healthy tissues with high ER expression during therapy with rintodestrant. This indicates that rintodestrant alters the kinetics of the tracer which could affect interpretation and quantification of ^{18}F-FES uptake. Of note, ≥6 days after ending treatment with rintodestrant, the biodistribution returned to baseline values, consistent with recovery of ER availability after wash-out of the drug.

Disclosure

The authors declare that they have no conflict of interest.

This study was financially supported by G1 Therapeutics Inc.

Acknowledgements

The authors would like to thank the patients for participating in this study. We would also like to thank the members of the department of Oncology and Radiology and Nuclear Medicine of Amsterdam UMC – location VUmc for tracer production and data acquisition.

Key points

Question: To describe the biodistribution of ^{18}F-FES in patients with metastatic ER+ breast cancer undergoing treatment with rintodestrant and understand the effect of rintodestrant on the biodistribution of the ^{18}F-FES tracer.

Pertinent findings: The biodistribution of the ^{18}F-FES tracer is altered in blood and in healthy tissues with high ER expression during therapy with rintodestrant. This indicates that rintodestrant affects the kinetics of the tracer which could affect interpretation and quantification of ^{18}F-FES uptake.

Implications for patient care: Changes in ER availability due to therapy that result in partial blockage or degradation of ER can potentially be quantified with ^{18}F-FES uptake. However, caution should be taken when doing so, since our data shows that during therapy the kinetics and biodistribution of the tracer are altered potentially affecting the interpretation.

References

1. Bray F, Ferlay J, Soerjomataram I, Siegel RL, Torre LA, Jemal A. Global cancer statistics 2018: GLOBOCAN estimates of incidence and mortality worldwide for 36 cancers in 185 countries. *CA Cancer J Clin.* 2018;68:394-424.
2. Weigelt B, Geyer FC, Reis-Filho JS. Histological types of breast cancer: how special are they? *Mol Oncol.* 2010;4:192-208.
3. Liao GJ, Clark AS, Schubert EK, Mankoff DA. 18F-Fluoroestradiol PET: current status and potential future clinical applications. *J Nucl Med.* 2016 Aug;57:1269-75.
4. Dees EC, Aftimos PG, Menke-van der Houven van Oordt, et al. Dose-escalation study of G1T48, an oral selective estrogen receptor degrader (SERD), in postmenopausal women with ER+/HER2- locally advanced or metastatic breast cancer (ABC). *Ann Oncol.* 2019;30:v104-142.
5. Venema CM, Appollonio G, Hospers GA, et al. Recommendations and technical aspects of 16alpha-[18F]fluoro-17beta-estradiol PET to image the estrogen receptor in vivo: the Groningen experience. *Clin Nucl Med.* 2016;41:844-851.
6. Sundararajan L, Linden HM, Link JM, Krohn KA, Mankhoff DA. 18F-Fluorestradiol. *Semin Nucl Med.* 2007;37:470-476.
7. Fowler AM, Clark AS, Katzenellenbogen JA, Linden HM, Desdashti F. Imaging diagnostic and therapeutic targets - steroid receptors in breast cancer. *J Nucl Med.* 2016;57:75S-80S.
8. Peterson LM, Kurland BF, Schubert EK, et al. A phase 2 study of 16α-[18 F]-fluoro-17β-estradiol positron emission tomography (FES-PET) as a marker of hormone sensitivity in metastatic breast cancer (MBC). *Mol. Imaging Biol.* 2014;16:431-440.
9. Van Kruchten M, De Vries EG, Glaudemans AW, et al. Measuring residual estrogen receptor availability during fulvestrant therapy in patients with metastatic breast cancer. *Cancer Discov.* 2015;5:72-81.
10. Dehdashti F, Flanagan FL, Mortimer JE, Katzenellenbogen JA, Welch MJ, Siegel BA. Positron emission tomographic assessment of “metabolic flare” to predict response of metastatic breast cancer to antiestrogen therapy. *Eur J Nucl Med.* 1999;26:51-56.
11. Linden HM, Stekhova SA, Link JM, et al. Quantitative fluoroestradiol positron emission tomography imaging predicts response to endocrine treatment in breast cancer. *J Clin Oncol.* 2006; 24:2793-2799.

12. Linden HM, Kurland BF, Peterson LM, et al. Fluoroestradiol (FES) positron emission tomography (PET) reveals differences in pharmacodynamics of aromatase inhibitors, tamoxifen, and fulvestrant in patients with metastatic breast cancer. *Clin Cancer Res.* 2011; 17:4799-4805.
13. Matej S, Browne JA. *Three Dimensional Image Reconstruction in Radiology and Nuclear Medicine: Performance of a fast maximum likelihood algorithm for fully-3D PET reconstruction.* Dordrecht, The Netherlands. Kluwer Academic Publishers; 1996:297–316.
14. Surti S, Kuhn A, Werner ME, Perkins AE, Kolthammer J, Karp JS. Performance of Philips Gemini TF PET/CT scanner with special consideration for its time-of-flight imaging capabilities. *J Nucl Med.* 2007;48:471–480.
15. Peterson LM, Kurland BF, Link JM, et al. Factors influencing the uptake of 18F-fluoroestradiol in patients with estrogen receptor positive breast cancer. *Nucl Med Biol.* 2011;38:969-978.
16. Boellaard R. Quantitative oncology molecular analysis suite: ACCURATE. *J Nucl Med.* 2018;59:1753.
17. Krak NC, Boellaard R, Hoekstra OS, Twisk JW, Hoekstra CJ, Lammertsma AA. Effects of ROI definition and reconstruction method on quantitative outcome and applicability in a response monitoring trial. *Eur J Nucl Med Mol Imaging*. 2005;32:294-301.
18. Hryb DJ, Khan MS, Romas AN, Rosner W. The control of the interaction of sex-hormone-binding globulin with its receptor by steroid hormones. *J Biol Chem.* 1990;265:6048-6054.
19. Stomati M, Hartmann B, Spinetti A, et al. Effects of hormonal replacement therapy on plasma sex hormone-binding globulin, androgen and insulin-like growth factor-1 levels in postmenopausal women. *J Endocrinol Invest.* 1996;19:535-541.
20. Lonning PE, Johannessen DC, Lien EA, Ekse D, Fotsis T, Adlercreutz H. Influence of tamoxifen on sex hormones, gonadotrophins and sex hormone binding globulin in postmenopausal breast cancer patients. *J Steroid Biochem Mol Biol.* 1995;52:491-496.
21. Mankoff DA, Tewson TJ, Eary JF. Analysis of blood clearance and labeled metabolites for the estrogen receptor tracer [F-18]-16α-Fluorestradiol (FES). Nucl. Med. Biol.I 1997;24:341-348.
22. Mankhoff DA, Peterson LM, Tewson TJ, et al. [18F]Fluoroestradiol radiation dosimetry in human PET studies. *J Nucl Med.* 2001;42:679-684.

23. Iqbal R, Menke-van der Houven van Oordt CW, Oprea-Lager DE, Booij J. [^{18}F]FES uptake in the pituitary gland and white matter of the brain. *Eur J Nucl Med Mol Imaging*. 2021. Epub ahead of print.
24. Human Protein Atlas. http://www.proteinatlas.org Accessed on June 2021.
25. Hua H, Zhang H, Kong Q, Jiang Y. Mechanisms for estrogen receptor expression in human cancer. *Exp Hematol Oncol.* 2018;7:24.

Figures

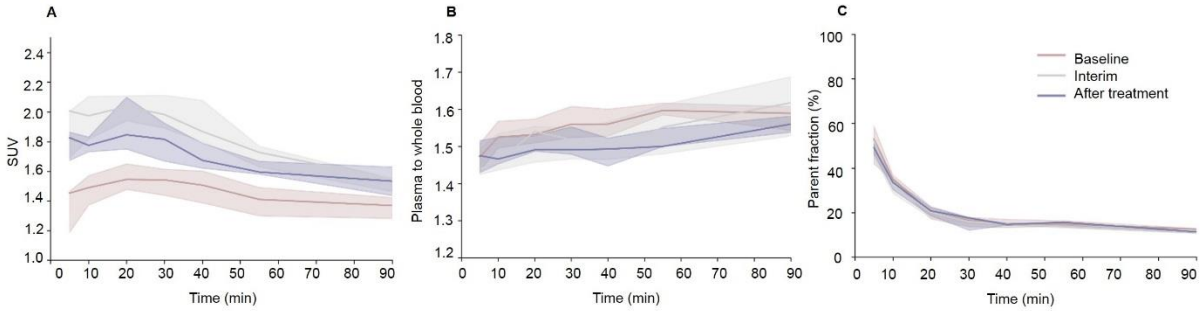

Figure 1. Venous blood sampling data of all patients obtained at the 3 different time-points. A) SUV whole blood data. B) Plasma-to-whole blood ratios. C) Parent fraction of ^{18}F-FES in plasma. Data represent the median of all values, with their corresponding interquartile ranges.

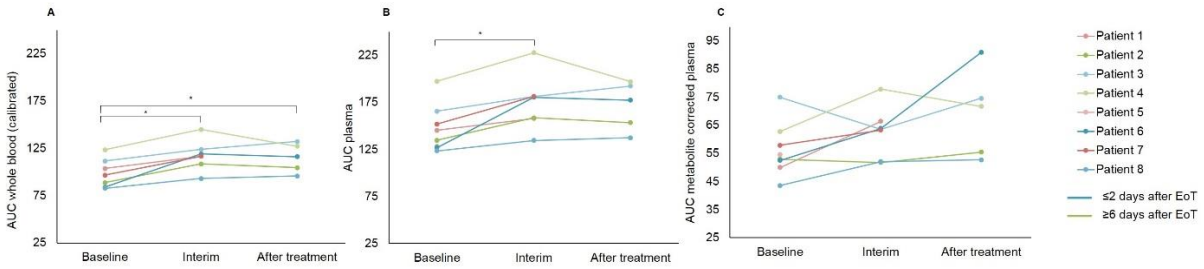

Figure 2. Tracer uptake in blood pool of each patient at the 3 different time-points. The whole blood calibrated with venous samples (A), plasma (B) and metabolite corrected plasma (C) input curves. All curves have been corrected for administered dose and weight. At time of progression, patients were scanned short (blue curves) or late (green curves) after end of treatment.

* P <0.05

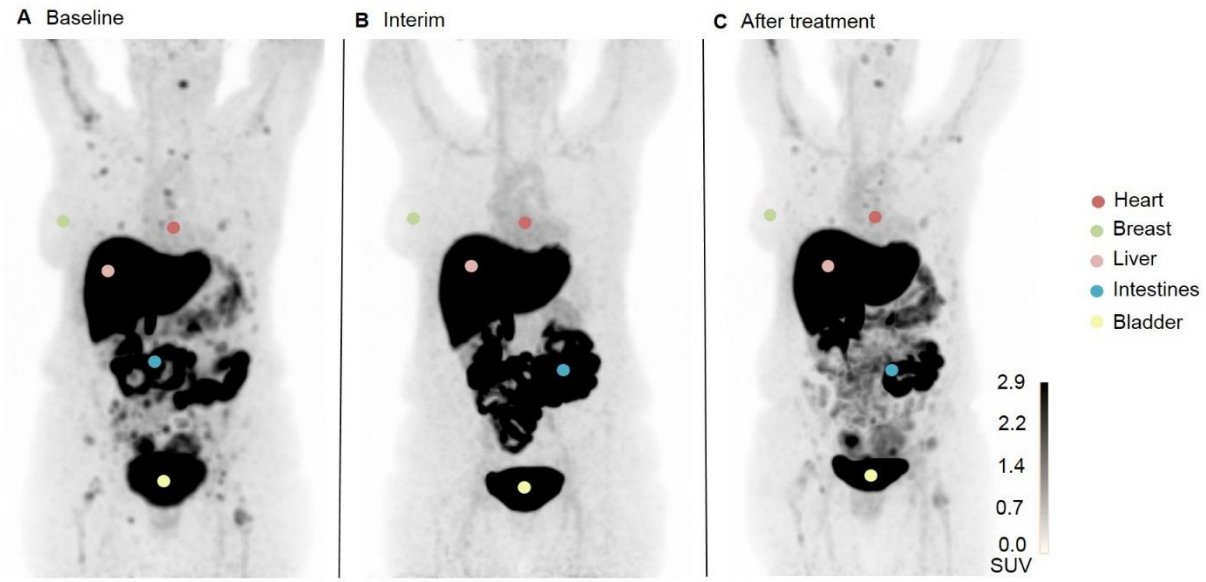

Figure 3. Visual assessment of ^{18}F-FES uptake in various healthy tissues in one patient at baseline (A), interim (B) and after treatment (C). This patient underwent the interim scan 10 days after end of treatment. The uterus, an ER expressing organ, is not visible in this Figure as it is located behind the bladder. Figures are maximal intensity projections.

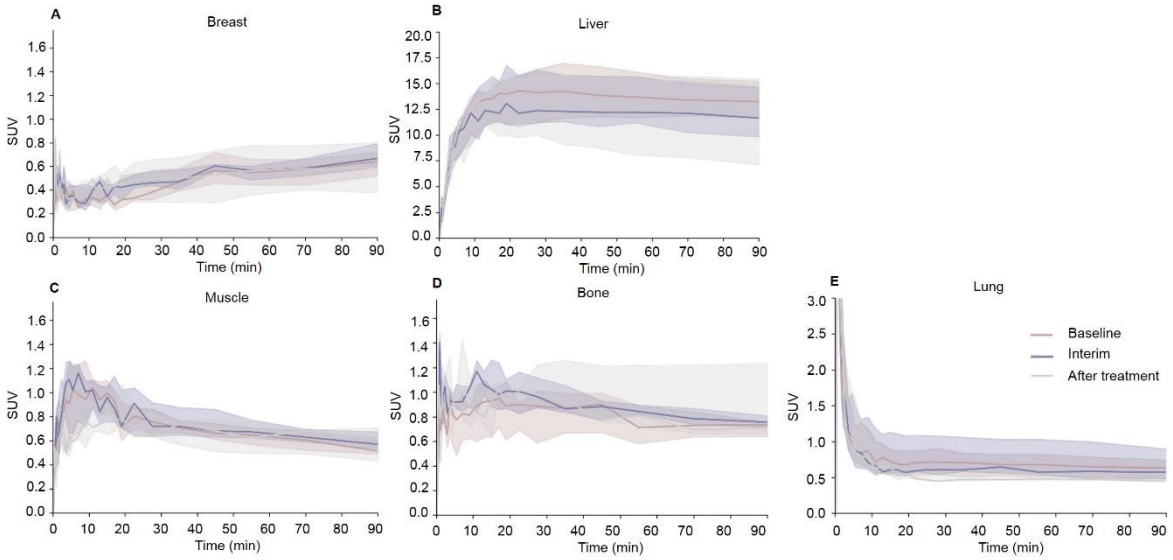

Figure 4. SUV time-activity curves (derived from the dynamic scans) for various healthy tissue regions (A: breast, B: liver, C: muscle, D: bone and E: lung) of all patients at the 3 different time-points. Curves represent the median of all values with their corresponding interquartile ranges.

Biodistribution of ^{18}F-FES in patients with metastatic ER+ breast cancer undergoing treatment with Rintodestrant (G1T48), a novel selective estrogen receptor degrader

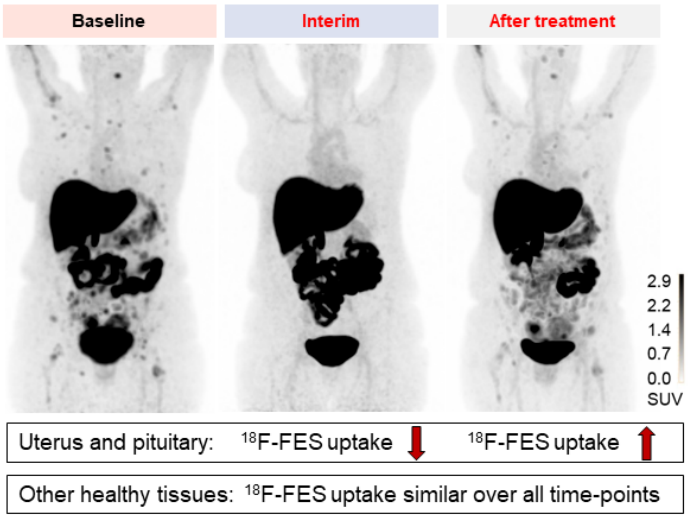

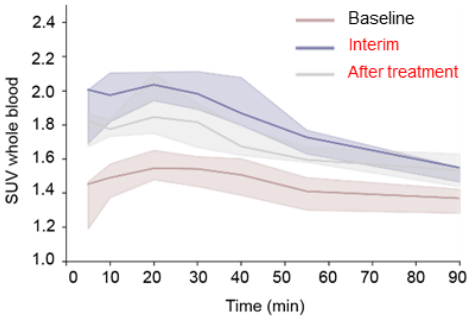

Conclusion: The biodistribution of ^{18}F-FES is altered in blood and in ER expressing healthy tissues during therapy with rintodestrant. This indicates that rintodestrant alters the kinetics of the tracer which could affect interpretation and quantification of ^{18}F-FES uptake.

Graphical Abstract

SUPPLEMENTAL DATA

	Number of patients (%) or mean (range)
Total patients included	8 (100.0)
Age (years)	63 (54-73)
Histological subtype	
- lobular	3 (37.5)
- ductal	5 (62.5)
Estrogen receptor	
- positive	8 (100.0)
Progesterone receptor	
- positive	8 (100.0)
HER2 receptor	
- negative	8 (100.0)
Treatments received	
- surgical resection	7 (87.5)
- radiotherapy	6 (75.0)
- chemotherapy	8 (100.0)
- endocrine therapy in metastatic setting	8 (100.0)
Rintodestrant therapy received*	7 (87.5)
- 400 mg	1 (12.5)
- 400 mg (cycle 1) and 800 mg afterwards**	1 (12.5)
- 600 mg	2 (25.0)
- 800 mg	1 (12.5)
- 1000 mg	2 (25.0)

SUPPLEMENTAL TABLE 1. Patient characteristics.

* 1 patient did not receive rintodestrant therapy as she was a screen failure, but she did undergo ^{18}F-FES PET/CT imaging at baseline which was used in this data set.

** 1 patient received 400 mg rintodestrant per day in the first cycle (i.e. 28 days) and this was increased to 800 mg per day afterwards to prevent under treatment, as it was found that higher doses have a better pharmacokinetic profile and are well tolerated.

Patients	Lines of chemotherapy	Lines of endocrine therapy in metastatic setting	Weight of patients			Rintodestrant dose received (mg)	Treatment duration (months)‡
			Baseline	Interim	After treatment†		
Patient 1*	1	3	111.1	114.0	NA	400	5.9
Patient 2	4	4	72.8	70.5	68.6	600	2.4
Patient 3	1	3	81.0	80.5	80.5	800	1.9
Patient 4	3	1	85.7	86.2	84.7	400 mg (cycle 1), 800 mg afterwards	1.7
Patient 5**	2	2	70.3	NA	NA	NA	NA
Patient 6	2	2	131.7	132.0	130.4	1000	4.1
Patient 7***	3	2	61.1	62.5	NA	1000	NA
Patient 8	2	2	63.5	65.5	58.8	600	8.2

SUPPLEMENTAL TABLE 2. Patient characteristics, classified accordingly per patient.

* Patient 1 did not receive the after treatment scan.

** Patient 5 is a screen failure and did therefore not receive rintodestrant.

*** Patient 7 is currently still receiving treatment.

† Patient weight was significantly different between baseline and after treatment, $P < 0.05$.

‡ Treatment duration is identical to the time to progression.

	Area under the curve (median ± IQR)			Area under the curve (median + range)	
SUV input functions	Baseline	Interim	After treatment***	After treatment, ≤2 days after EoT	After treatment, ≥6 days after EoT
Whole blood input, calibrated with venous blood samples	96.6 (86.3-123.3)	116.6 (112.5-144.9)*	110.3 (97.9-132.1)**	116.0 (95.7-132.1)	115.9 (104.-127.2)
Whole plasma input, calibrated with venous blood samples	145.3 (131.6-197.5)	180.4 (158.2-227.7)*	165.3 (141.4-197.0)	177.2 (137.4-192.4)	175.2 (153.5-197.0)
Metabolite corrected plasma input	54.6 (52.7-75.0)	63.6 (57.6-77.8)	63.6 (53.4-90.9)	74.6 (52.7-90.9)	63.6 (55.4-71.7)

SUPPLEMENTAL TABLE 3. Area under the curves of the various SUV input functions at baseline, interim and after treatment.

* Increase in AUC was significantly different between baseline and interim, P <0.05

** Increase in AUC was significantly different between baseline and after treatment, P <0.05

	Area under the curve (median ± IQR)		
Organs	Baseline	Interim	After treatment
Breast	25.3 (19.9-31.3)	27.0 (24.5-29.8)	26.7 (17.2-35.3)
Liver	705.2 (598.7-780.2)	593.4 (572.4-773.9)	736.2 (651.8-814.3)
Lung	39.0 (29.8-47.9)	32.6 (30.1-49.8)	28.0 (27.1-30.3)
Muscle	35.9 (34.4-37.5)	35.2 (32.5-44.2)	30.2 (27.2-35.1)
Bone	44.9 (29.0-45.3)	42.2 (38.7-44.4)	39.7 (35.4-47.3)

SUPPLEMENTAL TABLE 4. Area under the curves of the various SUV time-activity curves at baseline, interim and after treatment. For all organs, the differences in AUC were not significant ($P > 0.05$).

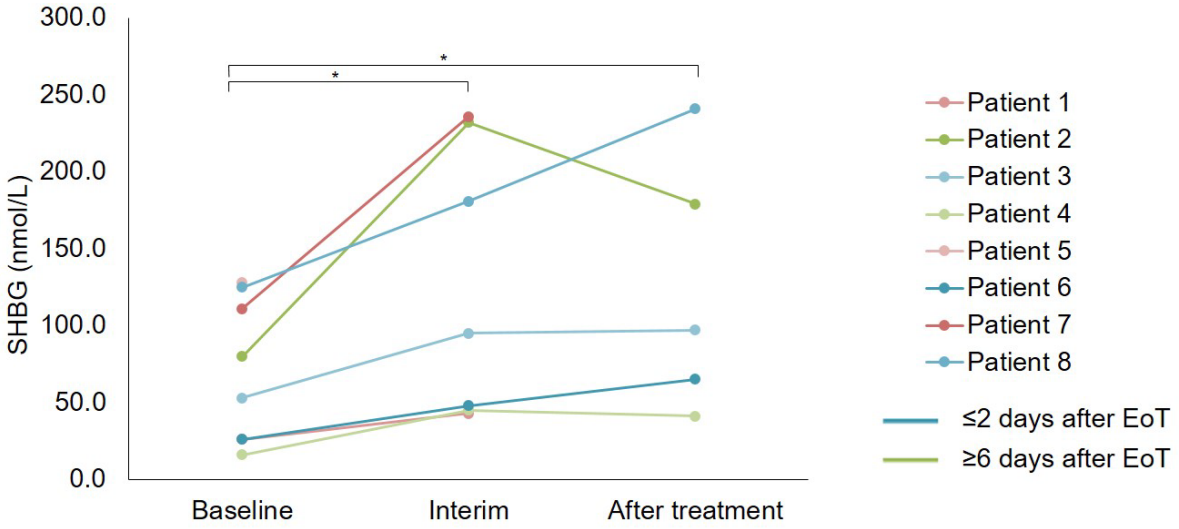

SUPPLEMENTAL FIGURE 1. Sex-hormone binding globuline levels in blood for each patient at baseline, interim and after treatment.

* P <0.05

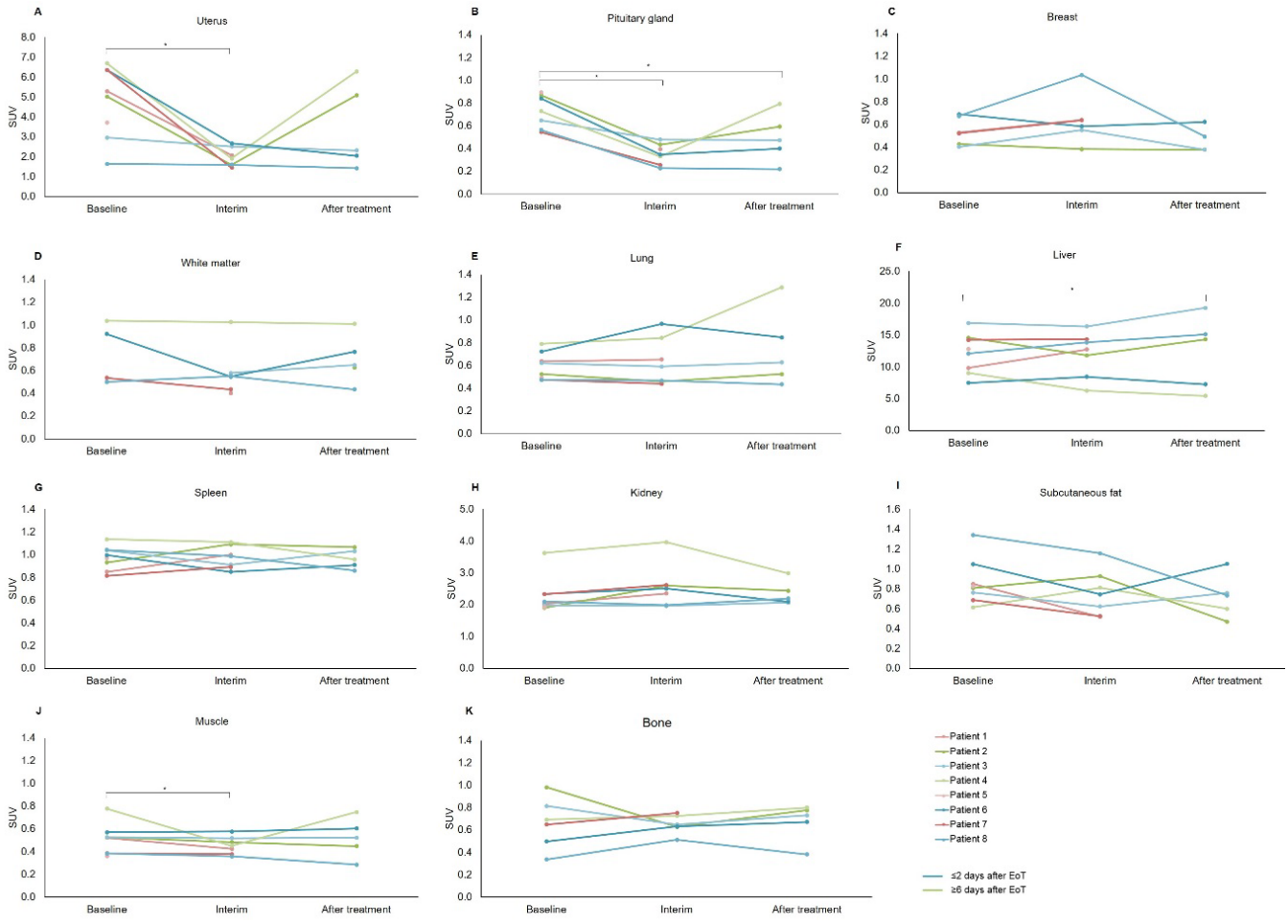

SUPPLEMENTAL FIGURE 2. Quantification of tracer uptake using SUV for various healthy tissues at the 3 different time-points. The after treatment scan was performed short (blue curves) or late (green curves) after end of treatment.

*P <0.05

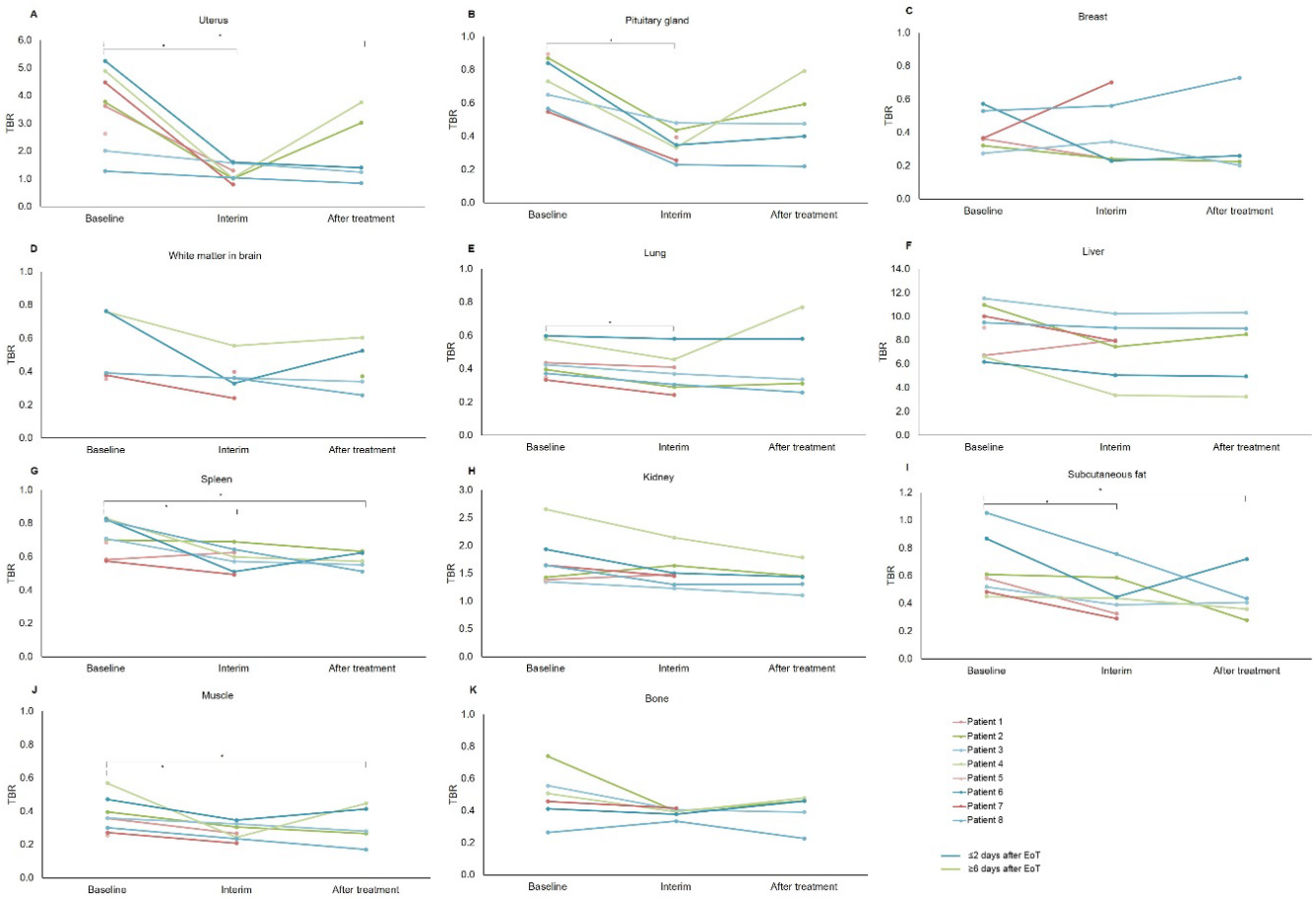

SUPPLEMENTAL FIGURE 3. Quantification of tracer uptake using TBR for various healthy tissues at the 3 different time-points. The after treatment scan was performed short (blue curves) or late (green curves) after end of treatment.

*P <0.05

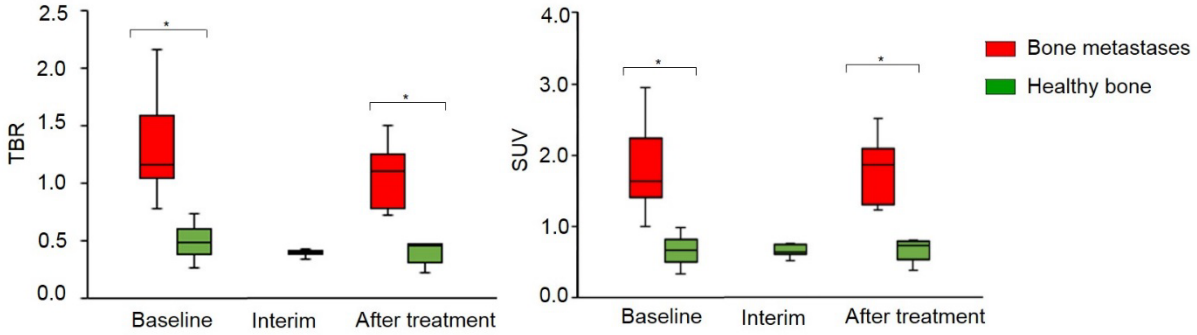

SUPPLEMENTAL FIGURE 4. Quantification of tracer uptake using SUV and TBR (median values with their interquartile range) in bone metastases and healthy bone at the 3 different time-points. At interim, no lesions could be visualized and quantified.

*P <0.003